

Experimental Realization of the Rabi-Hubbard Model with Trapped Ions

Q.-X. Mei^{1,*}, B.-W. Li^{1,*}, Y.-K. Wu^{1,*}, M.-L. Cai^{1,2}, Y. Wang¹, L. Yao^{1,2}, Z.-C. Zhou¹ and L.-M. Duan^{1,†}

¹Center for Quantum Information, Institute for Interdisciplinary Information Sciences, Tsinghua University, Beijing 100084, People's Republic of China

²HYQ Co., Ltd., Beijing, 100176, People's Republic of China

 (Received 9 November 2021; revised 26 March 2022; accepted 31 March 2022; published 22 April 2022)

Quantum simulation provides important tools in studying strongly correlated many-body systems with controllable parameters. As a hybrid of two fundamental models in quantum optics and in condensed matter physics, the Rabi-Hubbard model demonstrates rich physics through the competition between local spin-boson interactions and long-range boson hopping. Here, we report an experimental realization of the Rabi-Hubbard model using up to 16 trapped ions and present a controlled study of its equilibrium properties and quantum dynamics. We observe the ground-state quantum phase transition by slowly quenching the coupling strength, and measure the quantum dynamical evolution in various parameter regimes. With the magnetization and the spin-spin correlation as probes, we verify the prediction of the model Hamiltonian by comparing theoretical results in small system sizes with experimental observations. For larger-size systems of 16 ions and 16 phonon modes, the effective Hilbert space dimension exceeds 2^{57} , whose dynamics is intractable for classical supercomputers.

DOI: [10.1103/PhysRevLett.128.160504](https://doi.org/10.1103/PhysRevLett.128.160504)

The Hubbard model is a fundamental model in many-body physics, with rich physical phenomena arising from two competing effects: the on-site repulsion and the hopping between different sites [1]. One of its natural generalizations to the spin-boson coupled system is the Rabi-Hubbard (RH) model [2–4] where the on-site interaction is replaced by a quantum Rabi model Hamiltonian [5], a fundamental model in quantum optics describing the interaction of a spin with a bosonic mode. The RH model breaks the U(1) symmetry (particle number conservation) that appears in the other generalizations like the Bose-Hubbard model [6–8] and Jaynes-Cummings-Hubbard (JCH) model [9,10], and thus shows nontrivial distinctions in its ground state or general dynamics. Although important analytical and numerical progress has been achieved in understanding its properties [2–4,11–13], the RH model has not yet been realized in the cavity QED system where it was first proposed due to the experimental difficulty. This motivates one to realize and experimentally probe the RH model using other controllable physical systems through the idea of quantum simulation [14,15].

As the scale and the controllability of quantum devices develop, quantum simulation is becoming increasingly important in studying strongly correlated many-body systems [14,15]. As one of the leading platforms for quantum simulation, trapped ions possess a long coherence time, convenient initialization and readout [16]. Furthermore, the trapped ion system is intrinsically equipped with laser-coupled spin and bosonic degrees of freedom [16], which makes it an excellent candidate to simulate the light-matter interaction Hamiltonian. Previously, quantum simulation of

many-body spin models [17], the Dicke model [18], the quantum Rabi model of a single ion [19,20], and the JCH model for two [21,22] and three [23] ions have been demonstrated in this system. Here, we perform a quantum simulation of the RH model for the first time with up to 16 ions and explore its equilibrium phase transition [24] and quantum dynamical properties [25] using spin observables. Compared with the spin models where phonons are only virtually excited [17], our inclusion of phonon modes in the realization of the RH model greatly enlarges the effective dimension of the Hilbert space and thus demonstrates quantum simulation results that are intractable for the available classical computers.

Long-range Rabi-Hubbard model.—We use a chain of trapped $^{171}\text{Yb}^+$ ions to simulate the RH model. Our experimental setup is shown schematically in Fig. 1. The on-site quantum Rabi model Hamiltonian is generated through global bichromatic Raman laser beams [19,20] which couple the internal qubit states $|\downarrow\rangle \equiv |S_{1/2}, F=0, m_F=0\rangle$, $|\uparrow\rangle \equiv |S_{1/2}, F=1, m_F=0\rangle$ with the local transverse oscillation of the ions. Furthermore, the Coulomb interaction between the ions couples these local oscillation modes together and finally gives us an RH Hamiltonian

$$H = \sum_i \left[\frac{\omega_0}{2} \sigma_z^i + \omega_i a_i^\dagger a_i + g \sigma_x^i (a_i + a_i^\dagger) \right] + \sum_{i<j} t_{ij} (a_i^\dagger a_j + a_j^\dagger a_i), \quad (1)$$

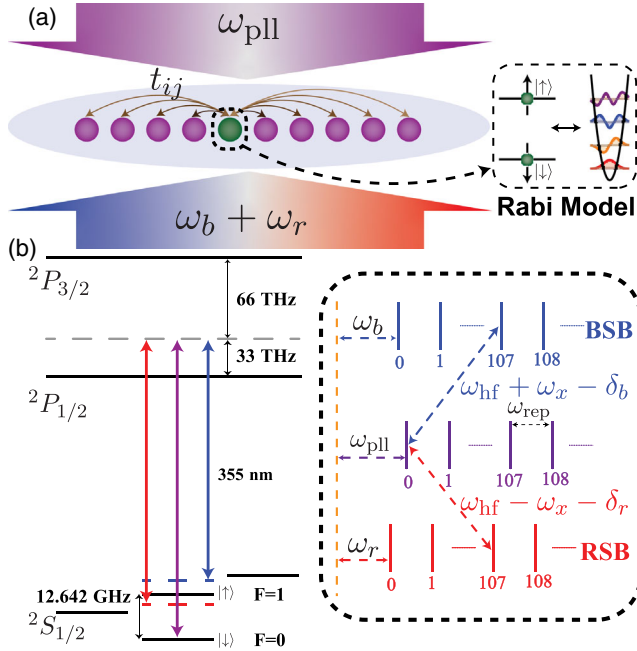


FIG. 1. Schematic of the experiment. (a) We use two global Raman laser beams to create a Rabi-Hubbard model Hamiltonian on an ion chain. Two frequency components are used to drive the blue and the red phonon sidebands (BSB and RSB) simultaneously. The frequency of the Raman pairs is locked by a phase-locked loop (PLL). The hopping rates among different sites t_{ij} are determined by the interion spacings, and the local quantum Rabi model Hamiltonian is controlled by the amplitudes and the frequencies of the driving lasers. (b) We use 355 nm pulsed laser beams with a frequency comb structure to bridge the Raman transitions of the qubits [31]. The large energy splitting of $\omega_{\text{hf}} = 2\pi \times 12.6$ GHz is covered by about 107 teeth of the frequency comb so we only need frequency shifts on the order of tens of MHz to set suitable detuning for the bichromatic Raman beams.

where σ_x^i and σ_z^i are Pauli operators for the spin i and a_i and a_i^\dagger the annihilation and creation operators of the corresponding local phonon mode. The spin frequency ω_0 is set by the detuning of the global bichromatic laser beams, the spin-phonon coupling g by the amplitudes, the phonon hopping term t_{ij} by the ion spacings, and the local phonon frequency ω_i by both the laser detuning and the Coulomb interaction and thus becomes inhomogeneous (see Supplemental Material for details [26]). Compared with the original RH model [2], our Hamiltonian has long-range hopping decaying inverse cubically with the distance.

Equilibrium quantum phase transition.—First, we study the quantum phase transition in this model by slowly tuning the spin-phonon coupling across the critical point, as shown in Fig. 2. The RH model has two distinct phases in its ground state [2]: at low phonon hopping rate and low spin-phonon coupling, the spin-spin correlation on distant sites vanishes, which is known as an incoherent phase; as the hopping and the coupling rates increase, long-range spin-spin correlation appears as the Z_2 symmetry spontaneously

breaks, and the system enters a coherent phase. Here, we start from zero spin-phonon coupling, for which the ground state can be easily prepared by sideband cooling of phonon modes into $|0\rangle$ and optical pumping of spins into $|\downarrow\rangle$. As the spin-phonon coupling g increases, the ground state phase transition can be understood qualitatively by a mean-field analysis (see Supplemental Material for details [26]). Diagonalizing the local phonon modes $\{a_i\}$ into collective modes $\{b_k\}$ and ignoring the quantum correlation between spin and phonon states, the only consistent solution at low g is $\langle\sigma_x^i\rangle = 0$ and $\langle b_k\rangle = 0$. As g goes up across a critical point $g_c^{\text{mf}} = \sqrt{\omega_0\delta_0}/2$ where δ_0 is the lowest frequency of the collective modes, $\langle b_0\rangle$ can acquire a nonzero value, which in turn leads to nonzero $\langle\sigma_x^i\rangle$ for each spin and nonzero $\langle b_k\rangle$ for other modes. In the experiment, we slowly tune up the coupling g following an exponential function $g(t) = (1 - e^{-t/\tau})g_{\text{max}}$ where $\tau = 1$ ms is the largest quench time and $(1 - 1/e)g_{\text{max}}$ above the critical point is the largest coupling rate. We expect the system to stay in the ground state adiabatically until close to the transition point where the energy gap closes in the thermodynamic limit. Nevertheless, this still allows us to observe the transition signal in the spin-spin correlation.

In our experiment, g is limited by the available laser power, so we set small $\delta_0 \approx 2\pi \times 2$ kHz for an achievable critical point. In Figs. 2(a)–2(e), we present the spin-spin correlation $C_{ij} \equiv \langle\sigma_x^i\sigma_x^j\rangle - \langle\sigma_x^i\rangle\langle\sigma_x^j\rangle$ for ion pairs with various distances in an $N = 10$ chain. At low coupling, ideally the spin-spin correlation is vanishingly small. In the experiment, we measure the spin-spin correlation by rotating $\sigma_\phi = \sigma_x \cos \phi + \sigma_y \sin \phi$ into the σ_z basis, scan the correlation with respect to ϕ , and then extract the oscillation amplitude of this curve as C_{ij} (see Supplemental Material [26]). While this process removes the sensitivity to the relative phase between the lab frame and the interaction picture of the RH Hamiltonian, it causes a systematic error when C_{ij} is close to zero since the fitted oscillation amplitude is always nonnegative: the statistical fluctuation or drift in the device parameters will now result in a measured positive correlation in the low- g regime, which is what we observe in these plots. As g rises near the mean-field transition point $g_c^{\text{mf}} = 2\pi \times 4.6$ kHz we observe a quick increase in the spin-spin correlations, which is a signature of the quantum phase transition. The experimental data agree well with the theoretical results calculated by the density-matrix-renormalization-group (DMRG) method [32] (solid lines), and the error comes from slow drifts in the trap frequencies (dashed lines for ± 300 Hz drifts), violation of the adiabatic condition, motional decoherence as well as SPAM errors (see Supplemental Material for details [26]). Furthermore, we see that the correlation in the coherent phase decays slowly with the distance and persists over half a chain, which is characteristic for this phase. In Fig. 2(f) we plot the experimental and

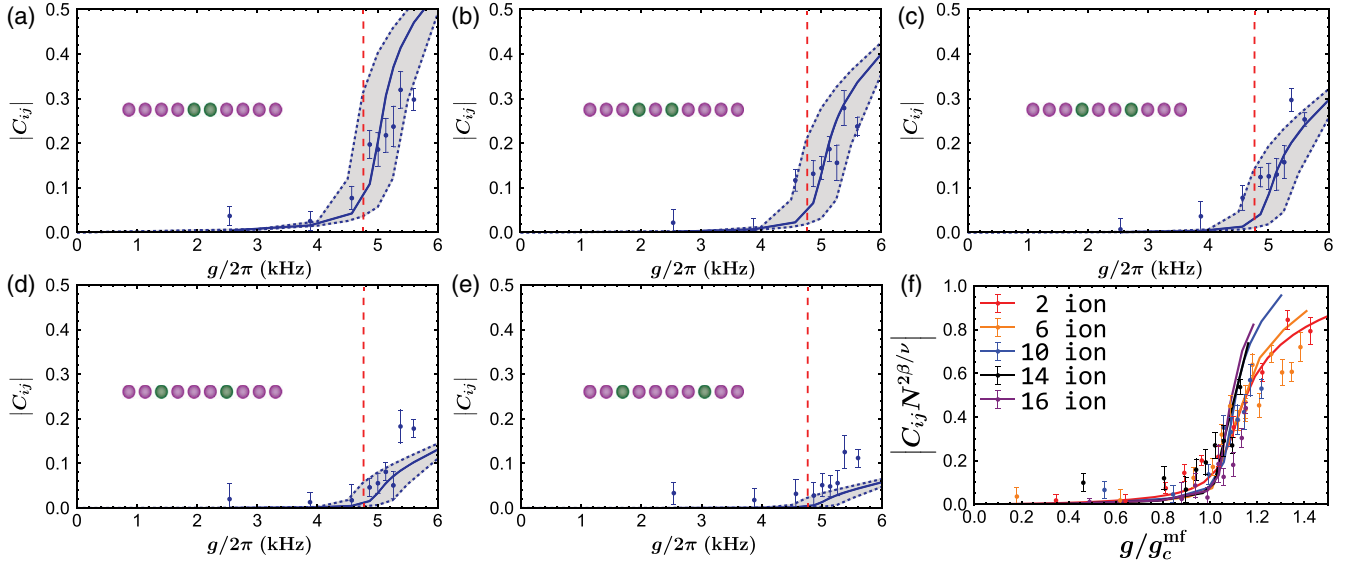


FIG. 2. Quantum phase transition under slow quench. We start from the ground state $|\Psi_0\rangle \equiv |\downarrow, 0\rangle^{\otimes N}$ with the on-site spin-phonon coupling $g = 0$, and then slowly tune up the coupling across the predicted critical point. (a)–(e) Spin-spin correlations $C_{ij} \equiv \langle \sigma_x^i \sigma_x^j \rangle - \langle \sigma_x^i \rangle \langle \sigma_x^j \rangle$ for various ion pairs in an $N = 10$ chain versus the coupling g after slow quench. For small g , the correlation remains close to zero apart from small detection errors; once g is tuned across a critical point (indicated by the vertical dashed line as the numerically computed value $g_c \approx 1.03g_c^{\text{mf}}$), the spin-spin correlation increases rapidly, which indicates a quantum phase transition. The solid line is the theoretical ground-state value from the DMRG calculation, and the shaded region between the dashed lines represents the theoretical results under a shift of ± 300 Hz in the trap frequency. (f) The nearest-neighbor spin-spin correlation for two central ions in a chain of 2–16 ions (dots with error bars representing one standard deviation) and the corresponding theoretical ground-state values from the DMRG calculation (solid lines). Here, we normalize the horizontal axis by the mean-field transition point g_c^{mf} , and scale the vertical axis by $N^{2\beta/\nu}$ where $\beta = 1/8$ and $\nu = 1$ are two critical exponents. Theoretically, the rise of the curves becomes sharper near the predicted transition point as N increases. Although this is less clear from the experimental data due to the noise and errors including the violation of adiabaticity and decoherence, the overall tendency between the theoretical and the experimental results still agrees with each other for different system sizes (see Supplemental Material for individual plots of each ion number N [26]).

the theoretical results for ion numbers ranging from 2 to 16. Although the current experimental accuracy is not enough for a finite size scaling analysis, we see that the experimental results are consistent with a transition point $g_c \approx 1.03g_c^{\text{mf}}$ predicted by the DMRG calculation with critical exponents $\beta = 1/8$ and $\nu = 1$. More details about this phase transition, choice of parameters, and adiabaticity can be found in Supplemental Material [26]. Also note that in Fig. 2(f), the range of data points for large N is narrower than those for small N . This is because for the experimental data we choose, g_c^{mf} is about 40% higher for the $N = 16$ case than for the $N = 2$ case so that the rescaled coupling g/g_c^{mf} decreases for the same spin-phonon coupling g . Besides, in the experiment we observe that the lifetime of the ion crystal under strong laser driving decreases with the increasing ion number, therefore for higher N we need to use smaller g .

Quantum dynamics.—Next, we consider nonequilibrium quantum dynamics of the RH Hamiltonian. As mentioned above, the ground-state properties of tens of ions can be computed using the DMRG method because of the low amount of entanglement in the one-dimensional system [32]. However, such methods will no longer be applicable

for quantum dynamics far from equilibrium. In Fig. 3 we initialize the system in $|\uparrow, 0\rangle^{\otimes N}$ through sideband cooling and optical pumping followed by a global Raman π pulse. Then, we turn on the RH Hamiltonian and measure the evolution of $\langle \sigma_z^i(t) \rangle$ for individual ions. In Figs. 3(a), 3(d), and 3(e), we see the measured dynamics agree well with the theoretical results from direct numerical integration of the Schrödinger equation for small system sizes. At small g , the spins are barely affected by the phonon coupling and hopping, and thus stay near $\langle \sigma_z^i(t) \rangle \approx 1$ (the lower experimental curves mainly come from SPAM errors); for larger g , the phonon modes become more important and we observe oscillatory or damping behavior in the spin dynamics. In Supplemental Material, we further show that this difference can be understood qualitatively from the stability of the system under the Holstein-Primakoff approximation [26]. In Figs. 3(b) and 3(f) we present the corresponding theoretical entanglement entropy between the left and the right halves of the chain (with both spin and phonon states included) and in Figs. 3(c) and 3(g) we plot the theoretical phonon numbers. All of these theoretical results demonstrate the explicit involvement of the phonon modes in the dynamics we are studying. (Note that an

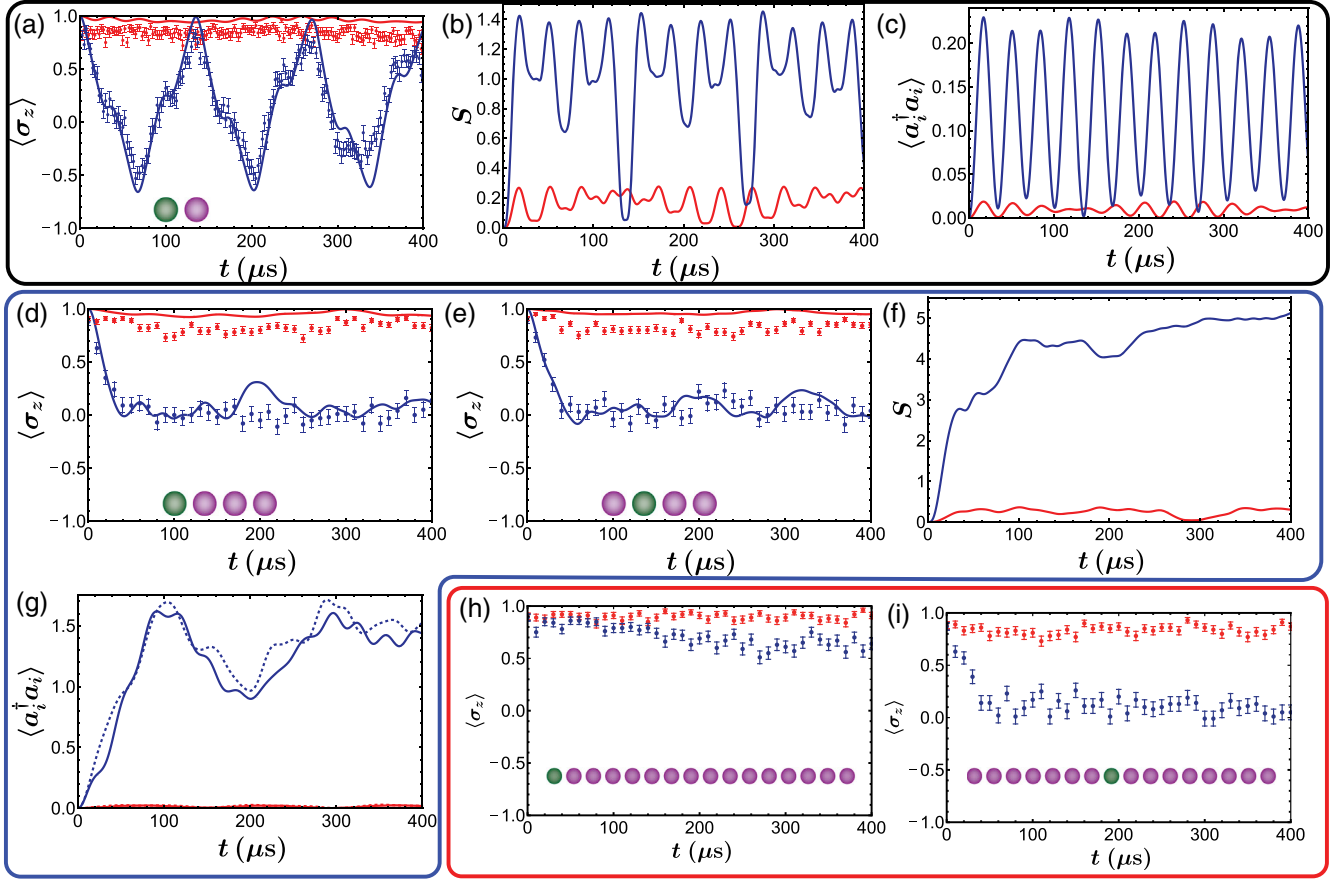


FIG. 3. Generic spin dynamics. We initialize the system in $|\uparrow, 0\rangle^{\otimes N}$, immediately turn on the RH Hamiltonian to evolve the system, and measure $\langle \sigma_z^i(t) \rangle$ of individual spins. (a) Measured data (dots with error bars representing one standard deviation) and theoretical results from numerically integrating the Schrödinger equation (solid lines) for $N = 2$ at $g = 2\pi \times 2$ kHz (red) and $2\pi \times 7$ kHz (blue). The two ions are symmetric and hence only one is plotted. (d),(e) Similar results for $N = 4$ at $g = 2\pi \times 1$ kHz (red) and $2\pi \times 6$ kHz (blue) for an ion on the edge and in the center, respectively. (b),(f) The corresponding evolution of entanglement entropy $S(t)$ for $N = 2$ and $N = 4$ between the left and the right halves of the chain (with both spin and phonon states included) under the two coupling strengths. (c),(g) Corresponding theoretical results for local phonon numbers $\langle a_i^\dagger(t)a_i(t) \rangle$. For $N = 4$ the solid and the dashed lines are for the central and the edge sites, respectively. (h),(i) The measured dynamics for the edge and the central spins of an $N = 16$ chain at $g = 2\pi \times 1$ kHz (red) and $2\pi \times 6$ kHz (blue).

entanglement entropy higher than $N/2$ proves that here the phonon states directly contribute to the entanglement and thus the dynamics are strikingly different from the Ising models simulated in earlier works [14] where the phonon states are adiabatically eliminated.) For an average phonon number around 1.5 as shown in Fig. 3(g), we need a cutoff of at least six for the local phonon number to capture the dynamics, thus the dimension of the system scales as $[2 \times (6 + 1)]^N$ (see Supplemental Material for details as well as for possible simplification using collective modes rather than local phonon modes [26]). On the other hand, the quick increase in the entanglement entropy clearly shows that here the matrix-product-state-based methods will not be applicable [32]. Therefore, the evolution of the RH model under the system size and the coupling strength achieved in this work, such as the spin dynamics in Figs. 3(h) and 3(i) for $N = 16$ ions, will generally be

difficult to simulate by classical supercomputers [33]: the dimension of $14^{16} \approx 2^{61}$ or, with the possible simplification in Supplemental Material using collective modes [26], of about 2^{57} , corresponds to 57 spins and even writing down such a pure state would take thousands of PB memories; besides, the phonon frequencies on the order of $2\pi \times 50$ kHz and the evolution time up to $400 \mu\text{s}$ require hundreds of layers of single-site and two-site unitary gates.

Conclusion.—In summary, we have reported the first experimental realization of the Rabi-Hubbard model and performed quantum simulation of both ground-state and dynamical properties of this model using a chain of up to 16 ions. We verify the simulation of the Hamiltonian by showing agreements between theories and experiments for quantum phase transition and for generic spin dynamics in small scales. We then perform quantum simulation in large scales that is generally intractable for classical

supercomputers. This experiment allows exploring rich ground-state and quantum dynamical properties of the RH model in future works, and showcases that the trapped ion system provides an ideal platform to probe and quantum simulate various spin-boson many-body models, which naturally arise and play important roles in a number of physics fields [2–4,9,10,34,35].

We thank X. Zhang and L. He for discussions. This work was supported by Tsinghua University Initiative Scientific Research Program, Beijing Academy of Quantum Information Sciences, National Key Research and Development Program of China, and Frontier Science Center for Quantum Information of the Ministry of Education of China. Y.-K. W. acknowledges support from Shuimu Tsinghua Scholar Program, International Postdoctoral Exchange Fellowship Program (Talent-Introduction Program) and the start-up fund from Tsinghua University.

*These authors contributed equally to this work.

[†]lmduan@tsinghua.edu.cn

- [1] H. Tasaki, Introduction to the Hubbard model, in *Physics and Mathematics of Quantum Many-Body Systems, Graduate Texts in Physics* (Springer International Publishing, Cham, 2020), pp. 305–339.
- [2] M. Schiró, M. Bordyuh, B. Öztop, and H. E. Türeci, Phase Transition of Light in Cavity QED Lattices, *Phys. Rev. Lett.* **109**, 053601 (2012).
- [3] M.-J. Hwang and M.-S. Choi, Large-scale maximal entanglement and Majorana bound states in coupled circuit quantum electrodynamic systems, *Phys. Rev. B* **87**, 125404 (2013).
- [4] G. Zhu, S. Schmidt, and J. Koch, Dispersive regime of the Jaynes-Cummings and Rabi lattice, *New J. Phys.* **15**, 115002 (2013).
- [5] P. Forn-Díaz, L. Lamata, E. Rico, J. Kono, and E. Solano, Ultrastrong coupling regimes of light-matter interaction, *Rev. Mod. Phys.* **91**, 025005 (2019).
- [6] M. P. A. Fisher, P. B. Weichman, G. Grinstein, and D. S. Fisher, Boson localization and the superfluid-insulator transition, *Phys. Rev. B* **40**, 546 (1989).
- [7] D. Jaksch, C. Bruder, J. I. Cirac, C. W. Gardiner, and P. Zoller, Cold Bosonic Atoms in Optical Lattices, *Phys. Rev. Lett.* **81**, 3108 (1998).
- [8] I. Bloch, J. Dalibard, and W. Zwerger, Many-body physics with ultracold gases, *Rev. Mod. Phys.* **80**, 885 (2008).
- [9] A. D. Greentree, C. Tahan, J. H. Cole, and L. C. L. Hollenberg, Quantum phase transitions of light, *Nat. Phys.* **2**, 856 (2006).
- [10] D. G. Angelakis, M. F. Santos, and S. Bose, Photon-blockade-induced Mott transitions and XY spin models in coupled cavity arrays, *Phys. Rev. A* **76**, 031805(R) (2007).
- [11] H. Zheng and Y. Takada, Importance of counter-rotating coupling in the superfluid-to-Mott-insulator quantum phase transition of light in the Jaynes-Cummings lattice, *Phys. Rev. A* **84**, 043819 (2011).
- [12] T. Flottat, F. Hébert, V. G. Rousseau, and G. G. Batrouni, Quantum Monte Carlo study of the Rabi-Hubbard model, *Eur. Phys. J. D* **70**, 213 (2016).
- [13] M. Schiró, C. Joshi, M. Bordyuh, R. Fazio, J. Keeling, and H. E. Türeci, Exotic Attractors of the Nonequilibrium Rabi-Hubbard Model, *Phys. Rev. Lett.* **116**, 143603 (2016).
- [14] I. M. Georgescu, S. Ashhab, and F. Nori, Quantum simulation, *Rev. Mod. Phys.* **86**, 153 (2014).
- [15] J. I. Cirac and P. Zoller, Goals and opportunities in quantum simulation, *Nat. Phys.* **8**, 264 (2012).
- [16] D. Leibfried, R. Blatt, C. Monroe, and D. Wineland, Quantum dynamics of single trapped ions, *Rev. Mod. Phys.* **75**, 281 (2003).
- [17] C. Monroe, W. C. Campbell, L.-M. Duan, Z.-X. Gong, A. V. Gorshkov, P. W. Hess, R. Islam, K. Kim, N. M. Linke, G. Pagano, P. Richerme, C. Senko, and N. Y. Yao, Programmable quantum simulations of spin systems with trapped ions, *Rev. Mod. Phys.* **93**, 025001 (2021).
- [18] A. Safavi-Naini, R. J. Lewis-Swan, J. G. Bohnet, M. Gärttner, K. A. Gilmore, J. E. Jordan, J. Cohn, J. K. Freericks, A. M. Rey, and J. J. Bollinger, Verification of a Many-Ion Simulator of the Dicke Model Through Slow Quenches across a Phase Transition, *Phys. Rev. Lett.* **121**, 040503 (2018).
- [19] D. Lv, S. An, Z. Liu, J.-N. Zhang, J. S. Pedernales, L. Lamata, E. Solano, and K. Kim, Quantum Simulation of the Quantum Rabi Model in a Trapped Ion, *Phys. Rev. X* **8**, 021027 (2018).
- [20] M.-L. Cai, Z.-D. Liu, W.-D. Zhao, Y.-K. Wu, Q.-X. Mei, Y. Jiang, L. He, X. Zhang, Z.-C. Zhou, and L.-M. Duan, Observation of a quantum phase transition in the quantum Rabi model with a single trapped ion, *Nat. Commun.* **12**, 1126 (2021).
- [21] K. Toyoda, Y. Matsuno, A. Noguchi, S. Haze, and S. Urabe, Experimental Realization of a Quantum Phase Transition of Polaritonic Excitations, *Phys. Rev. Lett.* **111**, 160501 (2013).
- [22] R. Ohira, S. Kume, K. Takayama, S. Muralidharan, H. Takahashi, and K. Toyoda, Blockade of phonon hopping in trapped ions in the presence of multiple local phonons, *Phys. Rev. A* **103**, 012612 (2021).
- [23] S. Debnath, N. M. Linke, S.-T. Wang, C. Figgatt, K. A. Landsman, L.-M. Duan, and C. Monroe, Observation of Hopping and Blockade of Bosons in a Trapped Ion Spin Chain, *Phys. Rev. Lett.* **120**, 073001 (2018).
- [24] S. Sachdev, *Quantum Phase Transitions* (Cambridge University Press, Cambridge, England, 2000).
- [25] A. Polkovnikov, K. Sengupta, A. Silva, and M. Vengalattore, Colloquium: Nonequilibrium dynamics of closed interacting quantum systems, *Rev. Mod. Phys.* **83**, 863 (2011).
- [26] See Supplemental Material at <http://link.aps.org/supplemental/10.1103/PhysRevLett.128.160504> for more details about experimental setup and scheme, experimental parameters, as well as detailed theoretical analysis for the quantum phase transition and quantum dynamics, which includes Refs. [27–30].
- [27] A. C. Lee, J. Smith, P. Richerme, B. Neyenhuis, P. W. Hess, J. Zhang, and C. Monroe, Engineering large Stark shifts for

- control of individual clock state qubits, *Phys. Rev. A* **94**, 042308 (2016).
- [28] N. Goldman and J. Dalibard, Periodically Driven Quantum Systems: Effective Hamiltonians and Engineered Gauge Fields, *Phys. Rev. X* **4**, 031027 (2014).
- [29] K. R. Brown, A. W. Harrow, and I. L. Chuang, Arbitrarily accurate composite pulse sequences, *Phys. Rev. A* **70**, 052318 (2004).
- [30] T. Holstein and H. Primakoff, Field dependence of the intrinsic domain magnetization of a ferromagnet, *Phys. Rev.* **58**, 1098 (1940).
- [31] R. Islam *et al.*, Beat note stabilization of mode-locked lasers for quantum information processing, *Opt. Lett.* **39**, 3238 (2014).
- [32] U. Schollwöck, The density-matrix renormalization group in the age of matrix product states, *Ann. Phys. (Amsterdam) January 2011 Special Issue*, **326**, 96 (2011).
- [33] F. Arute *et al.*, Quantum supremacy using a programmable superconducting processor, *Nature (London)* **574**, 505 (2019).
- [34] M. J. Hartmann, F. G. S. L. Brandão, and M. B. Plenio, Strongly interacting polaritons in coupled arrays of cavities, *Nat. Phys.* **2**, 849 (2006).
- [35] A. Kurcz, A. Bermudez, and J. J. García-Ripoll, Hybrid Quantum Magnetism in Circuit QED: From Spin-Photon Waves to Many-Body Spectroscopy, *Phys. Rev. Lett.* **112**, 180405 (2014).